Towards Sustainable Energy Systems: Multi-Objective Microgrid Sizing for Environmental and Economic Optimization

Lucas Zenichi Terada*, Juan Carlos Cortez*, Guilherme Souto Chagas*, Juan Camilo López†, and
Marcos J. Rider*

*School of Electrical and Computer Engineering (FEEC), Universidade Estadual de Campinas (UNICAMP), Brazil.
†Faculty of Electrical Engineering, Mathematics and Computer Science (EECMS), University of Twente, The Netherlands.
E-mails: lzenichi@ieee.org, juanc.cortez94@gmail.com, gschagas@unicamp.br,
j.c.lopezamezquita@utwente.nl, and mjrider@unicamp.br

Abstract—This paper proposes a new method for the multi-objective sizing of microgrids, which aims to minimize both the investment and operation costs, as well as the carbon footprint of their components and energy usage. The method employs Mixed Integer Linear Programming (MILP) and Pareto optimization to assess the balance between economic and environmental goals, constructed using the ϵ-constraint method. Additionally, the overall operation of a grid-connected microgrid is optimized considering unintentional islanding contingencies through a stochastic scenario-based mathematical programming model. Tests were conducted using data from CampusGrid, a real microgrid located at the University of Campinas (UNICAMP) in Brazil. The model determines the optimal size and type of Distributed Energy Resources (DERs), such as local Thermal Generation (TG), Photovoltaic (PV) systems, Battery Energy Storage Systems (BESSs), and load/generation curtailment requirements in islanded mode. For carbon-intensity comparison, a case study was conducted using attributes and parameters from the city of Beijing in China. The results provide valuable insights into the optimal sizing and configuration of microgrids, with an emphasis on cost-efficient and environmentally sounding energy solutions.

Index Terms—Greenhouse gas emissions, microgrid sizing, mixed-integer linear programming, multi-objective optimization, Pareto efficiency, renewable energy resources.

I. INTRODUCTION

With the increasing integration of Renewable Energy Sources (RESs) into the power grid, such as Photovoltaic (PV) and Wind Turbines (WT), microgrids have emerged as a key solution for effectively managing and harnessing these resources. Originally designed to address the energy needs of isolated areas without access to a main grid, microgrids have now evolved to enhance the reliability and sustainability of local power systems connected to the grid [1]. Microgrids can comprise a variety of Distributed Energy Resources (DERs), including RESs, storage systems, distributed generators, and controllable loads, all synergistically enhancing the flexibility, reliability, and efficiency of microgrids.

Non-renewable DERs are recognized for their higher reliability due to their dependence on fossil fuels, which are less susceptible to weather conditions. However, using fossil fuels contributes to Greenhouse Gas (GHG) emissions and entails substantial Operation and Maintenance (O&M) expenditures. On the contrary, RESs offer environmentally friendly alternatives but are inherently subject to stochastic fluctuations. As a solution, hybrid microgrids strategically integrate diverse energy resources and storage technologies, such as Battery Energy Storage System (BESS), to meet energy demands [2]. Skillful hybrid microgrid design yields a favorable cost-benefit equilibrium, as renewable energy production typically outperforms conventional energy production in terms of expenses. Despite RESs' higher initial investment costs compared to conventional distributed generation, the swift amortization of these upfront investments leads to a systematic reduction in reliance on non-renewable sources [1]. Although hybrid microgrids may exhibit higher initial costs compared to traditional power plants due to expensive storage units, their overall O&M costs remain lower [3].

In this scenario, the optimal design of a microgrid involves precisely determining optimal sizes and attributes for its DERs. As the optimization of microgrid sizing is a well-explored research subject, numerous studies have previously presented their findings in this area. In [1], the optimal sizing of a storage system under stochastic WT generation is proposed using Benders' decomposition. In [4], a two-stage method for optimizing the size and location of the DERs is proposed, considering on- and off-grid operational modes. The work presented in [5] proposes a reinforcement learning framework for optimal sizing and energy management of islanded microgrids that minimizes costs. [6] proposes an optimal sizing Mixed Integer Linear Programming (MILP) model for an islanded microgrid, which selects the best technology for storage batteries and WT from a set of commercial models.

NOMENCLATURE

Sets:

$\mathcal{B}, b$	Set/Index of available BESS technologies
$\mathcal{C}, c$	Set/Index of contingencies
$\mathcal{G}, g$	Set/Index of PV generation modules
$\mathcal{S}, s$	Set/Index of generation and demand scenarios
$\mathcal{T}, t$	Set/Index of time periods

Parameters:

Δt	Time step considered in the sizing problem [hours]
η_b^{char}	BESS charging efficiency
η_b^{dis}	BESS discharging efficiency
η_g^{PV}	PV generator efficiency
Γ_N	net present value
$\overline{E^{\text{BESS}}}$	Maximum installation energy capacity of BESS [kWh]
$\overline{P^{\text{EDS}}}$	Power limit that can be consumed from the EDS [kW]
$\overline{P^D}$	Maximum system load [kW]
$\overline{P^{\text{BESS}}}$	Maximum installation power capacity of BESS [kW]
$\overline{P^{\text{PV}}}$	Maximum installation capacity of PV system [kW]
$\overline{P^{\text{TG}}}$	Maximum operating power capacity of TG [kW]
$\pi_{s,c}$	Probability of scenario and contingency
EM_{MAX}	Maximum GHG emission [kgCO$_2$e]
m	Small value for accounting hours operated
c_t^{TG}	TG O&M cost [USD/kWh]
c_t^{EDS}	EDS operation cost [USD/kWh]
ci^{TG}	TG installation cost [USD/kW]
$ci_b^{\text{BESS,E}}$	BESS energy installation cost [USD/kWh]
$ci_b^{\text{BESS,P}}$	BESS power installation Cost [USD/kW]
ci_g^{PV}	PV installation cost [USD/kW]
D	Off-grid mode duration [hours]
DoD_b	BESS depth of discharge
e^{EDS}	GHG emission of EDS operation [kgCO$_2$e/kWh]
e^{TG}	GHG emissions of TG [kgCO$_2$e/kWh]
e_b^{BESS}	GHG emission of BESS operation [kgCO$_2$e/kWh]
e_g^{PV}	GHG emission of PV generation operation [kgCO$_2$e/kWh]
$f_{t,s}^D$	Load multiplication factor
$f_{t,s}^{\text{PV}}$	PV generation multiplication factor
M	Load curtailment cost [USD/kWh]
N_b^{cycle}	BESS lifetime in cycles
N_g^{PV}	PV life cycle [year]
Nh^{TG}	TG life cycle [hours]
PH	Planning horizon [years]
r	Annual interest rate
T	Time between investment and operation [years]

Variables:

α_b^{BESS}	Binary variable for BESS technology selection
α_g^{PV}	Binary variable for PV technology selection
$\chi_{t,s,c}^D$	Binary variable representing load curtailment
$\chi_{t,s,c}^{\text{PV}}$	Binary variable representing PV curtailment
$\delta_{t,s,c}^{\text{TG}}$	Binary variable of TG operating enable time
$\gamma_{t,s,c}^{\text{BESS,char}}$	Binary variable representing BESS charging
$\gamma_{t,s,c}^{\text{BESS,disc}}$	Binary variable representing BESS discharging
C	Total microgrid CAPEX [USD]
C_{BESS}	BESS investment cost [USD]
C_{PV}	PV system investment cost [USD]
C_{TG}	TG investment cost [USD]
EM	Total microgrid GHG emission [kgCO$_2$e]
EM_{BESS}	Total BESS GHG emissions [kgCO$_2$e]
EM_{EDS}	Total EDS GHG emission [kgCO$_2$e]
EM_{PV}	Total PV system GHG emissions [kgCO$_2$e]
EM_{TG}	Total TG GHG emission [kgCO$_2$e]
O	Total microgrid OPEX [USD]
O_{EDS}	EDS operating cost [USD]
O_{LC}	Load curtailment operating cost [USD]
O_{TG}	TG operating cost [USD]
R	Total microgrid RCV [USD]
R_{BESS}	BESS replacement cost [USD]
R_{PV}	PV system replacement cost [USD]
R_{TG}	TG replacement cost [USD]
$E_{\text{max}}^{\text{BESS}}$	Decision variable for installed BESS energy [kWh]
$E_{b,\text{max}}^{\text{BESS, lin}}$	Linear equivalence of installed BESS energy capacity [kWh]
$E_{t,s,c,b}^{\text{BESS,lin}}$	Linear equivalence of BESS operating energy [kWh]
$E_{t,s,c}^{\text{BESS}}$	BESS operating energy [kWh]
$P_{\text{max}}^{\text{BESS}}$	Decision variable for installed BESS power [kW]
$P_{\text{max}}^{\text{PV}}$	Decision variable for installed PV power [kW]
$P_{\text{max}}^{\text{TG}}$	Decision variable for installed TG power [kW]
$P_{t,s,c,\text{max}}^{\text{TG,lin}}$	Linear equivalence of TG installed capacity [kW]
$P_{b,\text{max}}^{\text{BESS, lin}}$	Linear equivalence of installed BESS power capacity [kW]
$P_g^{\text{PV,,}\alpha}$	Auxiliary variable for PV linear equivalence [kW]
$P_{t,s,c,b}^{\text{BESS,char,lin}}$	Linear equivalence of BESS charging power [kW]
$P_{t,s,c,b}^{\text{BESS,disc,lin}}$	Linear equivalence of BESS discharging power [kW]
$P_{t,s,c,g}^{\text{PV,lin}}$	Linear equivalent of PV operating power [kW]
$P_{t,s,c}^{\text{EDS,+}}$	Positive component of EDS operating power [kW]
$P_{t,s,c}^{\text{EDS,-}}$	Negative component of EDS operating power [kW]
$P_{t,s,c}^{\text{BESS,char}}$	BESS charging power [kW]
$P_{t,s,c}^{\text{BESS,disc}}$	BESS discharging power [kW]
$P_{t,s,c}^{\text{EDS}}$	EDS operating power [kW]
$P_{t,s,c}^{\text{PV}}$	PV system Operating power [kW]
$P_{t,s,c}^{\text{TG}}$	TG Operating power [kW]

Optimizing the design of microgrids is of utmost importance not only from an economic standpoint but also in terms of environmental sustainability. The dual objective of minimizing both the cost and GHG emissions of microgrids reflects the growing recognition that addressing climate change requires not only reducing reliance on fossil fuels but also ensuring the efficient sizing and utilization of RESs. This context propelled many previous studies. The work presented in [7] has a multi-objective optimization model that minimizes the costs of an off-grid system and the carbon emissions from the diesel generator using genetic algorithm (GA). In [8], a multi-objective optimization is done by minimizing the costs of an islanded microgrid using MILP, while the GHG emissions from a diesel generator are minimized using the ϵ-constraint method. In [9], [10], an off-grid system composed of PV, BESSs, and diesel generation is considered. [9] proposes a converged elephant herding optimization (cEHO) for minimizing the total system cost, while [10] uses a particle swarm optimization (PSO) method, and both use the ϵ-constraint method to minimize emissions from the diesel generator. A grid-connected energy system is modeled in [11], encompassing heating, cooling, and electrical subsystems. The study employs the non-dominated sorting genetic algorithm II (NSGA-II) to optimize the system reliability, annual expenditures, and emissions from fuel consumption within the microgrid and associated with grid electricity. In [12], a new self-adaptive multi-objective genetic algorithm (SAMOGA) is proposed for minimizing the component costs and carbon emissions from diesel generators on a grid-connected microgrid.

However, these prior studies exclusively account for carbon dioxide (CO_2) emissions coming from fossil fuel combustion. It is worth noting that while the power generated by RESs and stored within BESS does not trigger GHG emissions, a substantial energy quantity is consumed during the production, application, and disposal of the components of the system. In Life-Cycle Assessment (LCA) analyses, researchers evaluate

Reference	Technology choice	Fuel consumption emission model	DERs life-cycle emission model	On-grid model	Off-grid model	Model of RCV device	Solution method
[1]				✓			Benders' decomposition
[4]				✓	✓		MILP
[5]					✓	✓	Reinforcement Learning
[6]	✓				✓		MILP
[7]		✓			✓	✓	GA
[8]		✓			✓	✓	MILP / ϵ-Constraint
[9]		✓			✓	✓	cEHO / ϵ-Constraint
[10]		✓			✓	✓	PSO / ϵ-Constraint
[11]		✓		✓		✓	NSGA-II
[12]		✓			✓		SAMOGA
[13]		✓	✓		✓	✓	GA / MILP
This work	✓	✓	✓	✓	✓	✓	MILP / ϵ-Constraint

and assess the environmental impacts of products and services, comprehensively considering all their life-cycle processes. Many LCA studies have been carried out for different types of batteries [14]–[18] and PVs [19]–[21] to establish their equivalent carbon footprint. Considering LCA studies in the optimal design of microgrids is a novel paradigm for further reducing their environmental impact. In [13], a GA is used for sizing DERs that minimizes the cost and life-cycle emissions of all the components of an islanded microgrid. Table I summarizes the main attributes of the works mentioned above.

In this context, this paper proposes a novel holistic approach to address the multi-objective optimization of costs and GHG emissions in the design of microgrids. The model contemplates a grid-connected microgrid with PV, Thermal Generation (TG), and BESS, which is able to operate in islanded mode during contingencies of the main grid. Additionally, different scenarios of PV generation and load demands are considered while considering main-grid contingencies to guarantee system autonomy. This approach considers Capital Expenditures (CAPEX), Operating Expenses (OPEX), and Replacement Cost Value (RCV) for all components in the cost function. Furthermore, it integrates LCA of emissions from BESSs and PVs [13] as well as the equivalent carbon footprint per kWh from the imported energy and local TG. The proposed multi-objective optimization is represented using a MILP model and solved with the ϵ-constraint method to obtain an optimal Pareto front with the non-dominated solutions. In addition to finding the optimal sizing of the components, this model also decides the optimal choice between different technologies of PV panels and batteries available in the market. By encompassing these additional factors, this work provides a comprehensive contribution to optimizing grid-connected microgrid design, which, to the best of our knowledge, has not been addressed in previous works (see the last line in Table I). This approach not only promotes environmental sustainability but also ensures the economic viability of microgrids, contributing significantly to the transition to cleaner energy sources.

In summary, the main contribution of this paper is a new microgrid sizing optimization tool that contemplates: 1) life cycle emissions of PV panels and batteries; 2) multiple scenarios of local demand and PV generation; 3) off-grid operation due to contingencies of the main grid; 4) the RCVs of all

components in the cost function; 5) optimal choice between different technologies of batteries and PVs panels; 6) a holistic MILP model that allows an accurate assessment of the trade-off between overall costs and GHG emissions.

II. METHODOLOGY

The methodology of this paper focuses on utilizing MILP to address the complex task of sizing microgrids. Microgrids involving various DERs offer a promising solution for localized energy distribution. The complexity arises from the need to optimize the configuration of these resources while considering technical, economic, and environmental aspects. The presented methodology uses MILP to systematically determine optimal microgrid sizing by considering both discrete and continuous decision variables, enabling a comprehensive analysis of microgrid components and interactions.

A. MINLP formulation

The microgrid sizing problem becomes a Mixed-Integer Nonlinear Programming (MINLP) when the option to choose multiple technologies is introduced. This type of modeling utilizes the product of two variables: a binary variable representing the technology type and a continuous variable representing its capacity.

1) CAPEX model: The total CAPEX is defined by equation (1), which corresponds to the summation of investments resulting from the installation of BESS, TG, and PV systems.

$$C = C_{\text{BESS}} + C_{\text{PV}} + C_{\text{TG}} \tag{1}$$

The following equations model the installation investments for each component of the microgrid. Equation (2) shows the investment cost for BESS installation. Equation (3) calculates the installation cost of the PV system. Since this methodology involves the selection of different technologies, the nonlinearity of the problem appears in (2) and (3) due to the product between the binary variable that determines the type and size of the device to be installed. Lastly, (4) models the investment cost of TG installation.

$$C_{\text{BESS}} = \sum_{b \in \mathcal{B}} \left[\alpha_b^{\text{BESS}} \cdot (ci_b^{\text{BESS,P}} \cdot P_{\text{max}}^{\text{BESS}} + ci_b^{\text{BESS,E}} \cdot E_{\text{max}}^{\text{BESS}}) \right] \tag{2}$$

$$C_{\text{PV}} = \sum_{g \in \mathcal{G}} \left(ci_g^{\text{PV}} \cdot \alpha_g^{\text{PV}} \cdot P_{\text{max}}^{\text{PV}} \right) \tag{3}$$

$$C_{\text{TG}} = ci^{\text{TG}} \cdot P_{\text{max}}^{\text{TG}} \tag{4}$$

2) OPEX model: OPEX is defined by (5) and corresponds to the sum of operational costs represented by load curtailment and the energy supplied by the Energy Distributions System (EDS) and the TG system. Equations (6)–(8) model the individual costs, respectively.

$$O = O_{EDS} + O_{TG} + O_{LC} \tag{5}$$

$$O_{LC} = 365 \cdot \Gamma_N \cdot \Delta t \sum_{t \in \mathcal{T}} \sum_{s \in \mathcal{S}} \sum_{c \in \{0,\mathcal{C}\}} \left(M \cdot \pi_{s,c} \cdot f_{t,s}^D \cdot \overline{P^D} \cdot \chi_{t,s,c}^D \right) \tag{6}$$

$$O_{EDS} = 365 \cdot \Gamma_N \cdot \Delta t \sum_{t \in \mathcal{T}} \sum_{s \in \mathcal{S}} \sum_{c \in \{0,\mathcal{C}\}} \left(c_t^{EDS} \cdot \pi_{s,c} \cdot P_{t,s,c}^{EDS,+} \right) \tag{7}$$

$$O_{TG} = 365 \cdot \Gamma_N \cdot \Delta t \sum_{t \in \mathcal{T}} \sum_{s \in \mathcal{S}} \sum_{c \in \{0,\mathcal{C}\}} \left(c_t^{TG} \cdot \pi_{s,c} \cdot P_{t,s,c}^{TG} \right) \tag{8}$$

The operational costs represented in OPEX and RCV include a component that accounts for the net present value, aiming to bring equivalence to present costs. This component is defined according to equation (9) as outlined in reference [22].

$$\Gamma_N = \frac{1}{(1+r)^T} \cdot \frac{(1+r)^{PH} - 1}{r(1+r)^{PH}} \tag{9}$$

Regarding the probability parameter $(\pi_{s,c})$, its value is calculated based on the product between the probability of each PV level, load level, and off-grid mode, as described in (10), where $\sum_{s \in S, c \in \{0,C\}} \pi_{s,c} = 1$.

$$\pi_{s,c} = \pi(\text{PV level}) \times \pi(\text{Load level}) \times \pi(\text{off-grid}) \tag{10}$$

3) RCV model: In addition to considering investment and operational costs, this study incorporates the concept of RCV, which is quantified according to equation (11). RCV represents the total cost of replacing components installed at current prices to ensure that the capacity and functionality of the microgrid are maintained over time. This is calculated by summing up the RCV for each component, reflecting the financial provision required for future replacements essential to the system's sustainability.

$$R = R_{BESS} + R_{PV} + R_{TG} \tag{11}$$

Equation (12) shows the calculation of RCV for the BESS. The formulation considers the charge, discharge, and the device's number of cycles to determine the RCV over time. Equation (13) presents the RCV calculation for the TG. In this formulation, the binary variable $\delta_{t,s,c}^{TG}$ is used to account for the time the TG was operational. Therefore, the RCV formulation for the TG introduces an additional nonlinearity. Lastly, (14) demonstrates the RCV calculation for the PV based on the device lifespan.

$$R_{BESS} = 365 \cdot \Gamma_N \cdot \frac{\Delta t}{2} \cdot \sum_{t \in \mathcal{T}} \sum_{s \in \mathcal{S}} \sum_{c \in \{0,\mathcal{C}\}} \sum_{b \in \mathcal{B}} \left[\pi_{s,c} \cdot \alpha_b^{BESS} \cdot \frac{ci_b^{BESS}}{N_b^{cycles}} \cdot \right.$$
$$\left. \left(\eta_b^{char} \cdot P_{t,s,c}^{BESS,char} + \frac{1}{\eta_b^{disc}} \cdot P_{t,s,c}^{BESS,disc} \right) \right] \tag{12}$$

$$R_{TG} = 365 \cdot \Gamma_N \cdot \Delta t \sum_{t \in \mathcal{T}} \sum_{s \in \mathcal{S}} \sum_{c \in \{0,\mathcal{C}\}} \left(ci^{TG} \cdot \delta_{t,s,c}^{TG} \cdot \frac{P_{max}^{TG}}{Nh^{TG}} \right) \tag{13}$$

$$R_{PV} = \Gamma_N \sum_{g \in \mathcal{G}} \left(ci_g^{PV} \cdot \alpha_g^{PV} \cdot \frac{P_{max}^{PV}}{N_g^{PV}} \right) \tag{14}$$

4) Power flow and PV model: The power flow is modeled by (15), which accounts for all generations and demands from the perspective of the EDS.

$$P_{t,s,c}^{EDS} + P_{t,s,c}^{TG} + \sum_{g \in \mathcal{G}} \left[P_{t,s,c}^{PV} \cdot \alpha_g^{PV} \cdot (1 - \chi_{t,s,c}^{PV}) \right] + P_{t,s,c}^{BESS,disc} =$$
$$\overline{P^D} \cdot f_t^D \cdot \left(1 - \chi_{t,s,c}^D \right) + P_{t,s,c}^{BESS,char} \quad \forall t \in \mathcal{T}, s \in \mathcal{S}, c \in \{0,\mathcal{C}\} \tag{15}$$

The generated PV power is modeled in equation (16), which represents the product between the installed capacity and the generation profiles.

$$P_{t,s,c}^{PV} = P_{max}^{PV} \cdot f_{t,s,c}^{PV} \cdot \eta_g^{PV} \qquad \forall t \in \mathcal{T}, s \in \mathcal{S}, c \in \{0,\mathcal{C}\} \tag{16}$$

B. EDS and off-grid model

Equation (17) models the operational limits of the power supplied by the EDS, and (18) separates the positive and negative components of the EDS power. Moreover, (19) enforces the EDS power to be zero in case of off-grid mode operation for a duration of the contingency D, in hours.

$$-\overline{P^{EDS}} \le P_{t,s,c}^{EDS} \le \overline{P^{EDS}} \qquad \forall t \in \mathcal{T}, s \in \mathcal{S}, c \in \{0,\mathcal{C}\} \tag{17}$$

$$P_{t,s,c}^{EDS} = P_{t,s,c}^{EDS,+} - P_{t,s,c}^{EDS,-} \qquad \forall t \in \mathcal{T}, s \in \mathcal{S}, c \in \{0,\mathcal{C}\} \tag{18}$$

$$P_{t,s,c}^{EDS} = 0 \quad \forall\, t \in T, s \in S, c \in \{0,C\}\, |c \le t < c + D \text{ and } c > 0 \tag{19}$$

1) TG model: The operational limits of the TG were modeled by (20). The binary variable $\delta_{t,s,c}^{TG}$ in the lower and upper limits accounts for the periods of actual device operation, and P_{max}^{TG} is also a decision variable.

$$m \cdot \delta_{t,s,c}^{TG} \le P_{t,s,c}^{TG} \le P_{max}^{TG} \cdot \delta_{t,s,c}^{TG} \qquad \forall t \in \mathcal{T}, s \in \mathcal{S}, c \in \{0,\mathcal{C}\} \tag{20}$$

Where m corresponds to a very small value. This model was used to account for the number of times the TG was activated.

2) BESS model: The BESS model implemented in this paper considers nonlinearities due to the product between binary variables for technology selection and the maximum power and installation capacity of the BESS.

Equations (21)–(23) linearly model the charging and discharging of the BESS using binary variables.

$$0 \le P_{t,s,c}^{BESS,disc} \le P_{max}^{BESS} \cdot \gamma_{t,s,c}^{BESS,disc} \qquad \forall t \in \mathcal{T}, s \in \mathcal{S}, c \in \{0,\mathcal{C}\} \tag{21}$$

$$0 \le P_{t,s,c}^{BESS,char} \le P_{max}^{BESS} \cdot \gamma_{t,s,c}^{BESS,char} \qquad \forall t \in \mathcal{T}, s \in \mathcal{S}, c \in \{0,\mathcal{C}\} \tag{22}$$

$$\gamma_{t,s,c}^{BESS,disc} + \gamma_{t,s,c}^{BESS,char} \le 1 \qquad \forall t \in \mathcal{T}, s \in \mathcal{S}, c \in \{0,\mathcal{C}\} \tag{23}$$

Equations (24) and (25) restrict the operation of the BESS during off-grid mode periods to only supply what is demanded by the load.

$$0 \le P_{t,s,c}^{BESS,disc} \le P_{max}^{BESS} \cdot (1 - \chi_{t,s,c}^D) \qquad \forall t \in \mathcal{T}, s \in \mathcal{S}, c \in \{0,\mathcal{C}\} \tag{24}$$

$$0 \le P_{t,s,c}^{BESS,char} \le P_{max}^{BESS} \cdot (1 - \chi_{t,s,c}^D) \qquad \forall t \in \mathcal{T}, s \in \mathcal{S}, c \in \{0,\mathcal{C}\} \tag{25}$$

Equations (26) and (27) depict the BESS accumulated energy during the initial period and subsequent periods, respectively.

$$E_{t,s,c}^{BESS} = 0.5 \cdot E_{max}^{BESS} + \Delta t \sum_{b \in B} \left(\eta_b^{char} \cdot \alpha_b^{BESS} \cdot P_{t,s,c}^{BESS,char} \right.$$
$$\left. - \frac{1}{\eta_b^{disc}} \cdot \alpha_b^{BESS} \cdot P_{t,s,c}^{BESS,disc} \right) \qquad \forall\, t \in \mathcal{T}, s \in \mathcal{S}, c \in \{0,\mathcal{C}\}\, |t = 1 \tag{26}$$

$$E_{t,s,c}^{\text{BESS}} = E_{t-1,s,c}^{\text{BESS}} + \Delta t \sum_{b \in B} \left(\eta_b^{\text{char}} \cdot \alpha_b^{\text{BESS}} \cdot P_{t,s,c}^{\text{BESS,char}} \right.$$
$$\left. - \frac{1}{\eta_b^{\text{disc}}} \cdot \alpha_b^{\text{BESS}} \cdot P_{t,s,c}^{\text{BESS,disc}} \right) \qquad \forall t \in \mathcal{T}, s \in \mathcal{S}, c \in \{0, \mathcal{C}\} \,|\, t > 1 \quad (27)$$

Similar to the previous expressions, equations (28) and (29) implement the Depth of Discharge (DoD) models for the BESS.

$$- \sum_{b \in B} \left(DoD_b \cdot \alpha_b^{\text{BESS}} \cdot E_{\text{max}}^{\text{BESS}} \right) \leq E_{t,s,c}^{\text{BESS}} - 0.5 \cdot E_{\text{max}}^{\text{BESS}} \leq$$
$$\sum_{b \in B} \left(DoD_b \cdot \alpha_b^{\text{BESS}} \cdot E^{\text{BESS}} \right) \forall t \in \mathcal{T}, s \in \mathcal{S}, c \in \{0, \mathcal{C}\} \,|\, t = 1 \quad (28)$$

$$- \sum_{b \in B} \left(DoD_b \cdot \alpha_b^{\text{BESS}} \cdot E_{\text{max}}^{\text{BESS}} \right) \leq E_{t,s,c}^{\text{BESS}} - E_{t-1,s,c}^{\text{BESS}} \leq$$
$$\sum_{b \in B} \left(DoD_b \cdot \alpha_b^{\text{BESS}} \cdot E_{\text{max}}^{\text{BESS}} \right) \forall t \in \mathcal{T}, s \in \mathcal{S}, c \in \{0, \mathcal{C}\} \,|\, t > 1 \quad (29)$$

Equation (30) model the energy limits of the BESS based on the decision variable for maximum installed energy and the BESS off-grid scenario.

$$0 \leq E_{t,s,c}^{\text{BESS}} \leq E_{\text{max}}^{\text{BESS}} \qquad \forall t \in \mathcal{T}, s \in \mathcal{S}, c \in \{0, \mathcal{C}\} \quad (30)$$

Equation (31) ensures that the BESS has at least half of its capacity stored so that it can handle off-grid scenarios. Moreover, equation (32) ensures that the BESS profile of stored energy before an off-grid operation is equal to the on-grid profile.

$$E_{t,s,c}^{\text{BESS}} \geq 0.5 \cdot E_{\text{max}}^{\text{BESS}} \qquad \forall t \in \mathcal{T}, s \in \mathcal{S}, c \in \{0, \mathcal{C}\} \,|\, t < c \ \text{ or } \ c = 0 \quad (31)$$

$$E_{t,s,c}^{\text{BESS}} = E_{t,s,0}^{\text{BESS}} \qquad \forall \, t \in \, T, s \in \, S, c \in \{0, C\} \,|\, t < c \quad (32)$$

3) Technology additional constraints: Given that only one technology for the BESS and the PV system needs to be chosen, equations (33) and (34) ensure that this condition is satisfied.

$$\sum_{g \in G} \alpha_g^{\text{PV}} = 1 \qquad (33)$$

$$\sum_{b \in B} \alpha_b^{\text{BESS}} = 1 \qquad (34)$$

4) Operational constraints: Equations (35)–(38) impose upper limits on the decision variables of the capacities of the devices installed in the microgrid. These limits represent both the local installation capacities of the microgrid and the upper bounds for linearization techniques.

$$0 \leq P_{\text{max}}^{\text{PV}} \leq \overline{P^{\text{PV}}} \qquad (35)$$

$$0 \leq P_{\text{max}}^{\text{TG}} \leq \overline{P^{\text{TG}}} \qquad (36)$$

$$0 \leq P_{\text{max}}^{\text{BESS}} \leq \overline{P^{\text{BESS}}} \qquad (37)$$

$$0 \leq E_{\text{max}}^{\text{BESS}} \leq \overline{E^{\text{BESS}}} \qquad (38)$$

5) MINLP formulation: Once the cost and operation models of the components involved in microgrid sizing are defined, the formulation of the MINLP problem is given by (39). The formulation minimizes the total costs (CAPEX, OPEX, and RCV) subject to operational constraints.

$$\begin{cases} \quad \min \text{cost} = \{C + O + R\} \\ \text{Subject to:} \quad (1) - (38) \end{cases} \qquad (39)$$

C. Yearly GHG emission formulation

This paper takes into account the equivalent GHG emissions of the microgrid components, including the EDS, TG, BESS, and PV system. Equation (40) shows how the total annual emissions of the microgrid operation are calculated.

$$\text{EM} = \text{EM}_{\text{PV}} + \text{EM}_{\text{BESS}} + \text{EM}_{\text{EDS}} + \text{EM}_{\text{TG}} \qquad (40)$$

Equations (41) and (42) represent the proposed equivalent emissions in operation as outlined in [13], with modifications introduced by the nonlinear formulation of technology choice. Equations (43) and (44) directly convert the consumed energy into GHG emissions for the EDS and TG, respectively.

$$\text{EM}_{\text{PV}} = 365 \cdot \Delta t \sum_{t \in \mathcal{T}} \sum_{s \in \mathcal{S}} \sum_{c \in \{0, \mathcal{C}\}} \sum_{g \in \mathcal{G}} \left(e_g^{\text{PV}} \cdot P_{\text{max}}^{\text{PV}} \cdot f_{t,s,c}^{\text{PV}} \cdot \alpha_g^{\text{PV}} \right) \quad (41)$$

$$\text{EM}_{\text{BESS}} = 365 \cdot \frac{\Delta t}{2} \cdot \sum_{t \in \mathcal{T}} \sum_{s \in \mathcal{S}} \sum_{c \in \{0, \mathcal{C}\}} \sum_{b \in \mathcal{B}} \left[\pi_{s,c} \cdot \alpha_b^{\text{BESS}} \cdot \frac{e_b^{\text{BESS}}}{N_b^{\text{cycles}}} \right.$$
$$\left. \left(\eta_b^{\text{char}} \cdot P_{t,s,c}^{\text{BESS,char}} + \frac{1}{\eta_b^{\text{disc}}} \cdot P_{t,s,c}^{\text{BESS,disc}} \right) \right] \quad (42)$$

$$\text{EM}_{\text{EDS}} = 365 \cdot \Delta t \sum_{t \in \mathcal{T}} \sum_{s \in \mathcal{S}} \sum_{c \in \{0, \mathcal{C}\}} \left(e^{\text{EDS}} \cdot P_{t,s,c}^{\text{EDS},+} \right) \quad (43)$$

$$\text{EM}_{\text{TG}} = 365 \cdot \Delta t \sum_{t \in \mathcal{T}} \sum_{s \in \mathcal{S}} \sum_{c \in \{0, \mathcal{C}\}} \left(e^{\text{TG}} \cdot P_{t,s,c}^{\text{TG}} \right) \quad (44)$$

D. Linearization

The linear transformation involves using an equivalent formulation of the product of binary variables with continuous variables. The approach considered in this paper was based on the linearizations proposed in reference [23].

The equivalence for a linear model of the maximum PV capacity to be installed is represented by equation (45), considering PV curtailment. Additionally, constraints (47)–(49) are necessary to ensure linear equivalence.

$$\alpha_g^{\text{PV}} \cdot P_{\text{max}}^{\text{PV}} \cdot (1 - \chi_{t,s,c}^{\text{PV}}) \equiv P_{t,s,c,g}^{\text{PV,lin}} \qquad \forall g \in \mathcal{G} \quad (45)$$

In this case, finding an equivalence for the product between a continuous variable and two binary variables is necessary. Therefore, the equivalence needs to be done in two steps and with the assistance of two additional representative variables.

$$\alpha_g^{\text{PV}} \cdot P_{\text{max}}^{\text{PV}} \equiv P_g^{\text{PV},\alpha} \qquad \forall g \in \mathcal{G} \quad (46)$$

$$P_g^{\text{PV},\alpha} \leq P_{\text{max}}^{\text{PV}} \qquad \forall g \in \mathcal{G} \quad (47)$$

$$P_g^{\text{PV},\alpha} \leq \overline{P^{\text{PV}}} \cdot \alpha_g^{\text{PV}} \qquad \forall g \in \mathcal{G} \quad (48)$$

$$P_g^{\text{PV},\alpha} \geq P_{\text{max}}^{\text{PV}} + \overline{P^{\text{PV}}}(\alpha_g^{\text{PV}} - 1) \qquad \forall g \in \mathcal{G} \quad (49)$$

$$P_g^{\text{PV},\alpha} \cdot (1 - \chi_{t,s,c}^{\text{PV}}) \equiv P_{t,s,c,g}^{\text{PV, lin}} \qquad \forall t \in \mathcal{T}, s \in \mathcal{S}, c \in \{0, \mathcal{C}\}, g \in \mathcal{G} \quad (50)$$

$$P_{t,s,c,g}^{\text{PV, lin}} \leq P_g^{\text{PV},\alpha} \qquad \forall t \in \mathcal{T}, s \in \mathcal{S}, c \in \{0, \mathcal{C}\}, g \in \mathcal{G} \quad (51)$$

$$P_{t,s,c,g}^{\text{PV, lin}} \leq \overline{P^{\text{PV}}} \cdot (1 - \chi_{t,s,c}^{\text{PV}}) \qquad \forall t \in \mathcal{T}, s \in \mathcal{S}, c \in \{0, \mathcal{C}\}, g \in \mathcal{G} \quad (52)$$

$$P_{t,s,c,g}^{\text{PV, lin}} \geq P_g^{\text{PV},\alpha} - \overline{P^{\text{PV}}} \cdot \chi_{t,s,c}^{\text{PV}} \qquad \forall t \in \mathcal{T}, s \in \mathcal{S}, c \in \{0, \mathcal{C}\}, g \in \mathcal{G} \quad (53)$$

The product between the binary variable for technology choice and the nominal capacity of the BESS, both for power and energy, can be converted in a linear model using the equivalence presented in equations (54) and (58), respectively. To ensure equivalence, it must be added the constraints (55)–(57) and (59)–(61).

$$\alpha_b^{\text{BESS}} \cdot E_{\max}^{\text{BESS}} \equiv E_{b,\max}^{\text{BESS,lin}} \qquad\qquad \forall b \in \mathcal{B} \quad (54)$$

$$E_{b,\max}^{\text{BESS,lin}} \leq E_{\max}^{\text{BESS}} \qquad\qquad \forall b \in \mathcal{B} \quad (55)$$

$$E_{b,\max}^{\text{BESS,lin}} \leq \overline{E^{\text{BESS}}} \cdot \alpha_b^{\text{BESS}} \qquad\qquad \forall b \in \mathcal{B} \quad (56)$$

$$E_{b,\max}^{\text{BESS,lin}} \geq E_{\max}^{\text{BESS}} + \overline{E^{\text{BESS}}}(\alpha_b^{\text{BESS}} - 1) \qquad\qquad \forall b \in \mathcal{B} \quad (57)$$

$$\alpha_b^{\text{BESS}} \cdot P_{\max}^{\text{BESS}} \equiv P_{b,\max}^{\text{BESS,lin}} \qquad\qquad \forall b \in \mathcal{B} \quad (58)$$

$$P_{b,\max}^{\text{BESS,lin}} \leq P_{\max}^{\text{BESS}} \qquad\qquad \forall b \in \mathcal{B} \quad (59)$$

$$P_{b,\max}^{\text{BESS,lin}} \leq \overline{P^{\text{BESS}}} \cdot \alpha_b^{\text{BESS}} \qquad\qquad \forall b \in \mathcal{B} \quad (60)$$

$$P_{b,\max}^{\text{BESS,lin}} \geq P_{\max}^{\text{BESS}} + \overline{P^{\text{BESS}}}(\alpha_b^{\text{BESS}} - 1) \qquad\qquad \forall b \in \mathcal{B} \quad (61)$$

Similarly to the installed capacity, the powers and accumulated energy of the BESS during its operation should also be linearized. Equations (62), (66), and (70) demonstrate the equivalences that need to be applied in the formulation. Additionally, the constraints (63)–(65), (67)–(69), (71)–(73) enable the equivalences for the linearized model.

$$\alpha_b^{\text{BESS}} \cdot P_{t,s,c}^{\text{BESS,char}} \equiv P_{t,s,c,b}^{\text{BESS,char,lin}} \qquad \forall t \in \mathcal{T}, s \in \mathcal{S}, c \in \mathcal{C}, b \in \mathcal{B} \quad (62)$$

$$P_{t,s,c,b}^{\text{BESS,char,lin}} \leq P_{t,s,c}^{\text{BESS,char}} \qquad \forall t \in \mathcal{T}, s \in \mathcal{S}, c \in \mathcal{C}, b \in \mathcal{B} \quad (63)$$

$$P_{t,s,c,b}^{\text{BESS,char,lin}} \leq \overline{P^{\text{BESS}}} \cdot \alpha_b^{\text{BESS}} \qquad \forall t \in \mathcal{T}, s \in \mathcal{S}, c \in \mathcal{C}, b \in \mathcal{B} \quad (64)$$

$$P_{t,s,c,b}^{\text{BESS,char,lin}} \geq P_{t,s,c}^{\text{BESS,char}} + \overline{P^{\text{BESS}}}(\alpha_b^{\text{BESS}} - 1)$$
$$\forall t \in \mathcal{T}, s \in \mathcal{S}, c \in \mathcal{C}, b \in \mathcal{B} \quad (65)$$

$$\alpha_b^{\text{BESS}} \cdot P_{t,s,c}^{\text{BESS,disc}} \equiv P_{t,s,c,b}^{\text{BESS,disc,lin}} \qquad \forall t \in \mathcal{T}, s \in \mathcal{S}, c \in \mathcal{C}, b \in \mathcal{B} \quad (66)$$

$$P_{t,s,c,b}^{\text{BESS,disc,lin}} \leq P_{t,s,c}^{\text{BESS,disc}} \qquad \forall t \in \mathcal{T}, s \in \mathcal{S}, c \in \mathcal{C}, b \in \mathcal{B} \quad (67)$$

$$P_{t,s,c,b}^{\text{BESS,disc,lin}} \leq \overline{P^{\text{BESS}}} \cdot \alpha_b^{\text{BESS}} \qquad \forall t \in \mathcal{T}, s \in \mathcal{S}, c \in \mathcal{C}, b \in \mathcal{B} \quad (68)$$

$$P_{t,s,c,b}^{\text{BESS,disc,lin}} \geq P_{t,s,c}^{\text{BESS,disc}} + \overline{P^{\text{BESS}}}(\alpha_b^{\text{BESS}} - 1)$$
$$\forall t \in \mathcal{T}, s \in \mathcal{S}, c \in \mathcal{C}, b \in \mathcal{B} \quad (69)$$

$$\alpha_b^{\text{BESS}} \cdot E_{t,s,c}^{\text{BESS}} \equiv E_{t,s,c,b}^{\text{BESS,lin}} \qquad \forall t \in \mathcal{T}, s \in \mathcal{S}, c \in \mathcal{C}, b \in \mathcal{B} \quad (70)$$

$$E_{t,s,c,b}^{\text{BESS,lin}} \leq E_{t,s,c}^{\text{BESS}} \qquad \forall t \in \mathcal{T}, s \in \mathcal{S}, c \in \mathcal{C}, b \in \mathcal{B} \quad (71)$$

$$P_{t,s,c,b}^{\text{BESS,lin}} \leq \overline{E^{\text{BESS}}} \cdot \alpha_b^{\text{BESS}} \qquad \forall t \in \mathcal{T}, s \in \mathcal{S}, c \in \mathcal{C}, b \in \mathcal{B} \quad (72)$$

$$E_{t,s,c,b}^{\text{BESS,lin}} \geq E_{t,s,c}^{\text{BESS}} + \overline{E^{\text{BESS}}}(\alpha_b^{\text{BESS}} - 1)$$
$$\forall t \in \mathcal{T}, s \in \mathcal{S}, c \in \mathcal{C}, b \in \mathcal{B} \quad (73)$$

Finally, the product between the installed power of TG and the variable that tracks its operating time is linearized, as demonstrated by equations (74)–(77).

$$\delta_{t,s,c}^{\text{TG}} \cdot P_{\max}^{\text{TG}} \equiv P_{t,s,c,\max}^{\text{TG,lin}} \qquad\qquad \forall t \in \mathcal{T}, s \in \mathcal{S}, c \in \mathcal{C} \quad (74)$$

$$P_{t,s,c,\max}^{\text{TG,lin}} \leq P_{\max}^{\text{TG}} \qquad\qquad \forall t \in \mathcal{T}, s \in \mathcal{S}, c \in \mathcal{C} \quad (75)$$

$$P_{t,s,c,\max}^{\text{TG,lin}} \leq \overline{P^{\text{TG}}} \cdot \delta_{t,s,c}^{\text{TG}} \qquad\qquad \forall t \in \mathcal{T}, s \in \mathcal{S}, c \in \mathcal{C} \quad (76)$$

$$P_{t,s,c,\max}^{\text{PV,lin}} \geq P_{\max}^{\text{TG}} + \overline{P^{\text{TG}}}(\delta_{t,s,c}^{\text{TG}} - 1) \qquad\qquad \forall t \in \mathcal{T}, s \in \mathcal{S}, c \in \mathcal{C} \quad (77)$$

The formulation in equation (78) presents all the constraints and equivalences for the MILP modeling of microgrid sizing.

$$\begin{cases} \quad \min \text{cost} = \{C + O + R\} \\ \text{Subject to:} \\ \qquad (1)\text{–}(38), (47)\text{–}(49), (51)\text{–}(53) \\ \qquad (55)\text{–}(57), (59)\text{–}(61), (63)\text{–}(65) \\ \qquad (67)\text{–}(69), (71)\text{–}(73), (75)\text{–}(77) \\ \text{Apply equivalences } (45), (54), (58), (62), (66), (70) \text{ , and } (74) \end{cases}$$
$$(78)$$

Algorithm 1 Pareto front using the ϵ-constraint method

1: Define ΔEM   ▷ Small amount of emissions
2: **while** problem is feasible **do**
3:     Solve MILP model in (78)
4:     Calculate the maximum GHG emitted using (40) (a.k.a., EM$_{\max}$)
5:     Add the constraint EM $\leq$ EM$_{\max}$ − ΔEM
6:     Add the solution to the set of non-dominated results

E. Pareto Front

The Pareto front was constructed using the ϵ-constraint method, as described in Algorithm 1. This approach is a simple technique for multi-objective optimization where one objective is chosen to be optimized. The remaining objectives are considered in the form of adjustable constraints. The resulting set of non-dominated solutions is deployed in a so-called Pareto front, which is a decision-making tool that showcases the trade-off between objectives, in this case, total costs vs total emissions. A similar approach for a different optimization problem can be found in [24].

III. TEST CASE AND RESULTS

The microgrid size methodology proposed in this paper is applied specifically in the context of the University of Campinas, incorporating two technologies for both PV and BESS. This approach uses data relevant to the cities of Campinas, Brazil, and Beijing, China, to derive PV generation probabilities and energy pricing strategies. Table II outlines the PV technology data obtained from [13], [19], and the lithium BESS technology data from [25], [26]. The key parameters of the microgrid include a maximum demand ($\overline{P^D}$) of 500 kW. Operational limits are established as: $\overline{P^{\text{EDS}}}$ = 1 MW, $\overline{P^{\text{TG}}}$ = 500 kW, $\overline{P^{\text{PV}}}$ = 800 kW, $\overline{P^{\text{BESS}}}$ = 1000 kW, with a BESS capacity ($\overline{E^{\text{BESS}}}$) of 2000 kWh and C$_{\max}$ = of 2 MUSD.

The probabilities for the operational scenarios, presented in Table III, were determined with a focus on simulating a low-reliability microgrid environment. The distribution for off-grid modes was evenly set at four distinct times—3 a.m., 9 a.m., 3 p.m., and 9 p.m.—to ensure a balanced representation across the daily cycle. For the PV generation probabilities, historical global horizontal irradiance (GHI) data specific to the cities analyzed provided a factual basis sourced from

TABLE II
LI-ION BESS AND PV TECHNOLOGIES DATA

Type	ci [USD/kW]	η	DoD_b	GHG [kg/kWh]	N_b^{cycles}	N_g [year]
PV technologies data						
Perovskite	400	0.95		0.011		30
Si-PERC	310	0.95		0.018		30
BESS technologies data						
LFP	815	0.93	0.88	147	3600	
LTO	1,553	0.94	0.99	266	10000	

TABLE III
PROBABILITY CONSIDERED FOR EACH SCENARIO AND OFF-GRID MODE

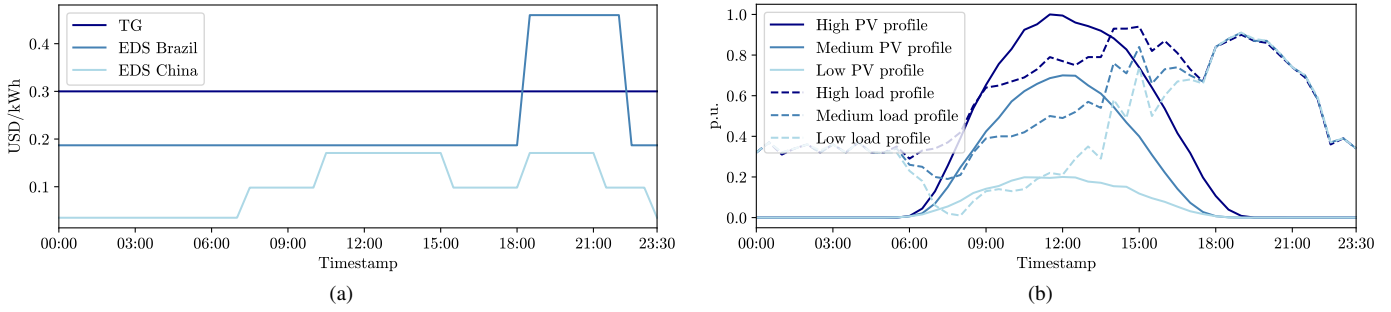|	Low	Medium	High	On-grid	Off-grid
Campinas PV	0.014	0.293	0.693		
Beijing PV	0.093	0.485	0.422		
Load profile	0.330	0.330	0.340		
Off-grid mode				0.900	0.100

Fig. 1. Optimization problem parameters: (a) Brazil and China EDS energy cost and TG cost. (b) PV and Load Scenarios.
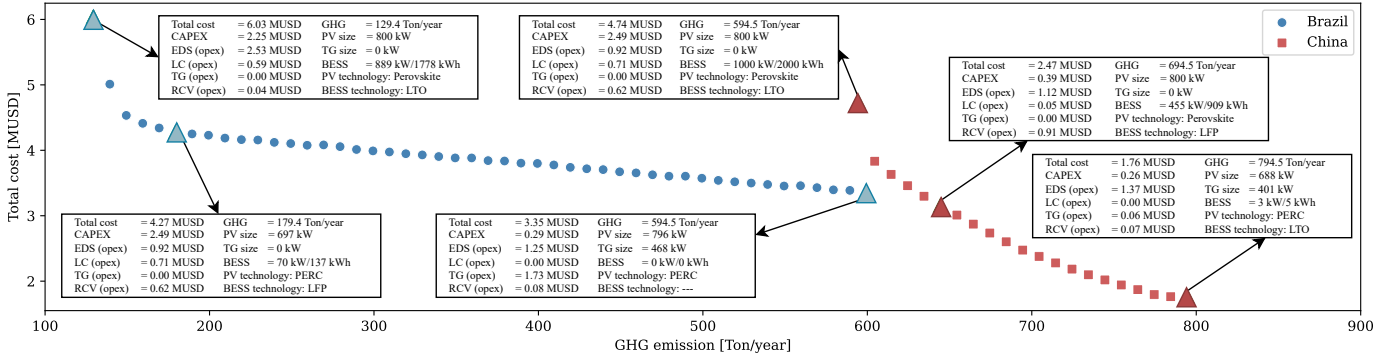

Fig. 2. Optimization problem results. Pareto front obtained from Campinas COE and Brazilian average EDS GHG emission; and from Beijing COE and Chinese average EDS GHG emission.

Solcast. This data-driven approach for PV generation aligns with the empirical nature of the scenarios explored. A comparative analysis across two systems with different GHI profiles highlighted the impact of these probability parameters on the solution outcomes, underscoring the importance of tailored probabilistic inputs in modeling microgrid performance.

Regarding the TG, the following parameters were considered: ci^{TG} = 100 USD/kW and N_h^{TG} = 50,000 hours. Concerning operational costs, the load curtailment considered was 1 USD/kWh, and the costs of the TG and EDS are depicted in Fig. 1a based on references [13], [27], [28].

The GHG emissions considered for the imported energy from the EDS in the cities of Campinas and Beijing were 102 gCO_2e/kWh and 531 gCO_2e/kWh, respectively. These values were obtained from [29] and correspond to the countries' average GHG emissions in 2022. The GHG emissions from the operation of the TG were considered to be 800 gCO_2e/kWh, based on [13].

Regarding the other parameters, the off-grid mode time duration was 3 hours, the planning horizon was set to 10 years, the time between investment and operation was 1 year, and Δt was 30 minutes. The annual interest rate was equal to 1%.

The simulations considered the COE and PV generation scenarios for each city, with Fig. 2 illustrating the combined Pareto curves for Beijing and Campinas, showcasing the total cost associated with various GHG emission levels, and including representative samples detailing cost and sizing. The limits of the curve are set by the infeasibility due to the maximum sizing constraints for PV and BESS. A notable observation across both scenarios was the necessity for at least one technology swap to adhere to GHG emission limits

during the construction of the Pareto curve. The disparity between the curves, particularly in the total cost to achieve equivalent emissions, primarily derives from the GHG emissions associated with imported energy from the EDS, with Beijing's equivalent emissions from imported energy being approximately five times higher than Campinas', underscoring the need for a more significant investment in DER in Beijing to match the GHG emissions levels attainable in Campinas.

Although time-intensive, the construction of Pareto curves aligns with the strategic nature of microgrid planning in tackling the computational demands of microgrid planning. This long-term approach mitigates the emphasis on computational speed compared to operational contexts. Efficiency gains for larger systems or with additional technologies can be realized through strategic pre-processing, such as excluding less viable technologies early on. This refined focus ensures practicality in planning without compromising computational depth.

Finally, Fig. 3 shows three examples of operation resulting from the highlighted midpoint at Pareto's curve from the Campinas scenario. It is worth noting that there was even a PV curtailment for the contingency at 9 a.m. to ensure compliance with the grid operational limits.

IV. CONCLUSION

This paper proposes a Mixed Integer Linear Programming (MILP) model for microgrid sizing that considers both grid-connected and islanded operation modes, the Replacement Cost Value (RCV) of Distributed Energy Resources (DERs), the selection of technologies for Battery Energy Storage System (BESS) Systems Photovoltaic (PV) panels, as well as modeling Greenhouse Gas (GHG) emissions from microgrid components. By incorporating GHG emissions modeling from
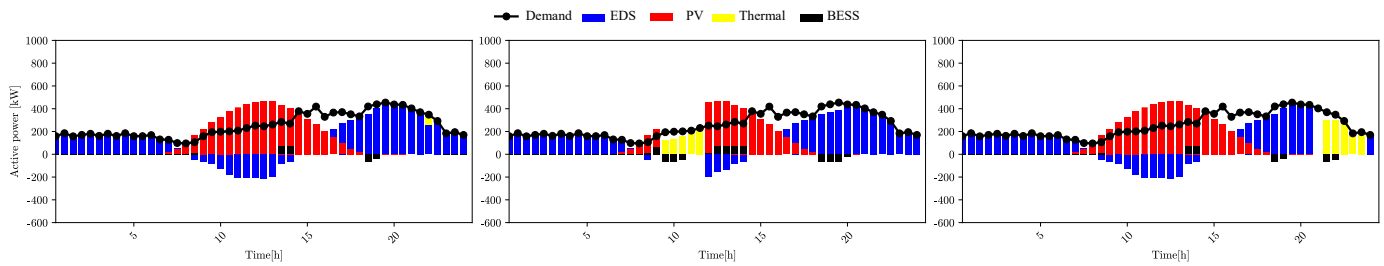
Fig. 3. Operation obtained for Brazil's highlighted midpoint of the Pareto curve. Left graph: full on-grid operation. Middle figure: microgrid islanding operation at 9 a.m. Right figure: Microgrid islanding operation at 9 p.m.

microgrid components, Pareto fronts of annual GHG emissions and total cost were obtained, considering aspects of both Campinas in Brazil and Beijing in China. The evolution of the Pareto front demonstrated that a slight increase in investment has the potential to significantly reduce global GHG emissions. Finally, the methodology successfully identified solutions with different technologies along the Pareto front.

REFERENCES

[1] M. A. Abdulgalil, M. Khalid, and F. Alismail, "Optimizing a Distributed Wind-Storage System Under Critical Uncertainties Using Benders Decomposition," *IEEE Access*, vol. 7, pp. 77 951–77 963, 2019.

[2] A. L. Bukar and C. W. Tan, "A review on stand-alone photovoltaic-wind energy system with fuel cell: System optimization and energy management strategy," *Journal of Cleaner Production*, vol. 221, pp. 73–88, Jun. 2019.

[3] S. Singh, D. W. Gao, and J. Giraldez, "Cost analysis of renewable energy-based microgrids," in *2017 North American Power Symposium (NAPS)*, Sep. 2017, pp. 1–4.

[4] K. V. Santos, L. Higino Silva Santos, N. Bañol Arias, J. C. López, M. J. Rider, and L. C. P. d. Silva, "Optimal Sizing and Allocation of Distributed Energy Resources in Microgrids Considering Internal Network Reinforcements," *Journal of Control, Automation and Electrical Systems*, vol. 34, no. 1, pp. 106–119, Feb. 2023.

[5] Y. Khawaja, I. Qiqieh, J. Alzubi, O. Alzubi, A. Allahham, and D. Giaouris, "Design of cost-based sizing and energy management framework for standalone microgrid using reinforcement learning," *Solar Energy*, vol. 251, pp. 249–260, 2023.

[6] A. Naderipour, H. Saboori, H. Mehrjerdi, S. Jadid, and Z. Abdul-Malek, "Sustainable and reliable hybrid AC/DC microgrid planning considering technology choice of equipment," *Sustainable Energy, Grids and Networks*, vol. 23, p. 100386, Sep. 2020.

[7] P. Premadasa, C. Silva, D. Chandima, and J. Karunadasa, "A multi-objective optimization model for sizing an off-grid hybrid energy microgrid with optimal dispatching of a diesel generator," *Journal of Energy Storage*, vol. 68, p. 107621, 2023.

[8] H. Akter, H. O. R. Howlader, A. Y. Saber, P. Mandal, H. Takahashi, and T. Senjyu, "Optimal Sizing of Hybrid Microgrid in a Remote Island Considering Advanced Direct Load Control for Demand Response and Low Carbon Emission," *Energies*, vol. 14, no. 22, p. 7599, Jan. 2021.

[9] M. A. Ashraf, Z. Liu, A. Alizadeh, S. Nojavan, K. Jermsittiparsert, and D. Zhang, "Designing an optimized configuration for a hybrid PV/Diesel/Battery Energy System based on metaheuristics: A case study on Gobi Desert," *Journal of Cleaner Production*, vol. 270, p. 122467, Oct. 2020.

[10] F. Fodhil, A. Hamidat, and O. Nadjemi, "Potential, optimization and sensitivity analysis of photovoltaic-diesel-battery hybrid energy system for rural electrification in Algeria," *Energy*, vol. 169, pp. 613–624, Feb. 2019.

[11] Y. Wang, X. Wang, H. Yu, Y. Huang, H. Dong, C. Qi, and N. Baptiste, "Optimal design of integrated energy system considering economics, autonomy and carbon emissions," *Journal of Cleaner Production*, vol. 225, pp. 563–578, Jul. 2019.

[12] X. Zhu, C. Peng, and H. Geng, "Multi-objective sizing optimization method of microgrid considering cost and carbon emissions," in *2022 4th International Conference on Smart Power & Internet Energy Systems (SPIES)*, 2022, pp. 2278–2283.

[13] F. Boutros, M. Doumiati, J.-C. Olivier, I. Mougharbel, and H. Kanaan, "New modelling approach for the optimal sizing of an islanded microgrid considering economic and environmental challenges," *Energy Conversion and Management*, vol. 277, p. 116636, Feb. 2023.

[14] V. B. Costa, R. S. Capaz, and B. D. Bonatto, "Small steps towards energy poverty mitigation: Life cycle assessment and economic feasibility analysis of a photovoltaic and battery system in a Brazilian indigenous community," *Renewable and Sustainable Energy Reviews*, vol. 180, p. 113266, Jul. 2023.

[15] R. Yudhistira, D. Khatiwada, and F. Sanchez, "A comparative life cycle assessment of lithium-ion and lead-acid batteries for grid energy storage," *Journal of Cleaner Production*, vol. 358, p. 131999, Jul. 2022.

[16] A. Bouter and X. Guichet, "The greenhouse gas emissions of automotive lithium-ion batteries: a statistical review of life cycle assessment studies," *Journal of Cleaner Production*, vol. 344, p. 130994, Apr. 2022.

[17] F. Arshad, J. Lin, N. Manurkar, E. Fan, A. Ahmad, M.-u.-N. Tariq, F. Wu, R. Chen, and L. Li, "Life Cycle Assessment of Lithium-ion Batteries: A Critical Review," *Resources, Conservation and Recycling*, vol. 180, p. 106164, May 2022.

[18] J. F. Peters and M. Weil, "Providing a common base for life cycle assessments of Li-Ion batteries," *Journal of Cleaner Production*, vol. 171, pp. 704–713, Jan. 2018.

[19] N. Bartie, L. Cobos-Becerra, F. Mathies, J. Dagar, E. Unger, M. Fröhling, M. A. Reuter, and R. Schlatmann, "Cost versus environment? combined life cycle, techno-economic, and circularity assessment of silicon-and perovskite-based photovoltaic systems," *J. of Industrial Ecology*, 2023.

[20] D. Colarossi, E. Tagliolini, A. Amato, and P. Principi, "Life cycle assessment and circularity evaluation of a PV panel integrated with phase change material," *Renewable Energy*, vol. 201, pp. 150–156, Dec. 2022.

[21] T. H. Mehedi, E. Gemechu, and A. Kumar, "Life cycle greenhouse gas emissions and energy footprints of utility-scale solar energy systems," *Applied Energy*, vol. 314, p. 118918, May 2022.

[22] A. Tabares, J. F. Franco, M. Lavorato, and M. J. Rider, "Multistage long-term expansion planning of electrical distribution systems considering multiple alternatives," *IEEE Transactions on Power Systems*, vol. 31, no. 3, pp. 1900–1914, 2016.

[23] M. Asghari, A. M. Fathollahi-Fard, S. M. J. Mirzapour Al-e hashem, and M. A. Dulebenets, "Transformation and Linearization Techniques in Optimization: A State-of-the-Art Survey," *Mathematics*, vol. 10, no. 2, p. 283, Jan. 2022.

[24] J. F. Franco, M. J. Rider, M. Lavorato, and R. Romero, "A mixed-integer lp model for the optimal allocation of voltage regulators and capacitors in radial distribution systems," *International Journal of Electrical Power & Energy Systems*, vol. 48, pp. 123–130, 2013.

[25] T. Le Varlet, O. Schmidt, A. Gambhir, S. Few, and I. Staffell, "Comparative life cycle assessment of lithium-ion battery chemistries for residential storage," *Journal of Energy storage*, vol. 28, p. 101230, 2020.

[26] C. E. Reviews. (2023) Detailed home solar battery guide. Accessed on: 2023-08-22. [Online]. Available: https://www.cleanenergyreviews.info/blog/home-solar-battery-cost-guide

[27] N. Solar. (2023) Cpfl electricity prices 2023. Accessed on: 2023-08-22. [Online]. Available: https://www.ngsolar.com.br/single-post/preco-kwh-cpfl

[28] T. P. G. of Beijing Municipality. (2023) Beijing sales electricity tariff. Accessed on: 2023-08-22. [Online]. Available: https://www.beijing.gov.cn/zhengce/zhengcefagui/202012/W020201201332914812668.pdf

[29] O. W. in Data. (2023) Carbon intensity of electricity. Accessed on: 2023-08-22. [Online]. Available: https://ourworldindata.org/grapher/carbon-intensity-electricity?tab=table